Available online at www.sciencedirect.com
SCIENCE DIRECT®
PERGAMON
Polyhedron 22 (2003) 3065–3072
POLYHEDRON
www.elsevier.com/locate/poly

Ultrathin micropatterned porphyrin films assembled via zirconium phosphonate chemistry

Aaron M. Massari, Richard W. Gurney, Matt D. Wightman, Chien-Hao Kane Huang, SonBinh T. Nguyen, Joseph T. Hupp *

Department of Chemistry and the Institute for Nanotechnology, Northwestern University, 2145 Sheridan Road, Evanston, IL 60208-3113, USA

Received 10 July 2002; accepted 15 August 2002

Abstract

The synthesis of a phosphonic-acid-functionalized porphyrin is presented and a procedure for the reproducible assembly of the porphyrins into thin films on glass or conductive glass surfaces is described. The assembly scheme, which utilizes established zirconium phosphonate (ZrP) chemistry, yields highly oriented films (normal to the surface) of well-defined thicknesses. In the lateral direction (plane parallel to the surface) the porphyrins interact by edge-on-edge contact and are characterized by significant porosity. Electrochemical redox-probe experiments indicate the existence of openings or pores of several angstroms in width in both monolayer and multilayer ZrP porphyrin films. Micropatterned versions of the films, capable of diffracting visible light, have also been prepared and have been used for the direct evaluation of film thicknesses via atomic force microscopy.

Keywords: Porphyrins; Thin films; Zirconium phosphonates; Diffraction gratings

1. Introduction

Directed assembled and layer-by-layer assembled thin films have been studied for a variety of applications ranging from electroluminescence [1–3] to second-harmonic generation [4–6]. Although film preparation is often conceptually simple, the fabrication of stable and ordered multilayer films has often proved challenging. Repetitive zirconium phosphonate (ZrP) linkage formation [7–9] offers one solution. The success of this approach stems from the low solubility of ZrP compounds, despite the high solubility of tetravalent zirconium and diphosphonic acids. A further attraction – a consequence of the stepwise nature of the assembly process – is that film thicknesses can be controlled with outstanding precision. Mallouk and co-workers, for example, have utilized ZrP layer-by-layer assembly for the preparation of geometrically well-defined electrically insulating films [10], single electron-counting capacitors [11], and chromophoric multilayers which display inter- and intralayer electron and energy transfer behavior [12,13]. Our interests center on *porous* thin films – especially porphyrinic films – that can function as molecular sieves [14], selective catalysts, chemical sensors [15], or chromophores for liquid-junction solar cells.

Herein we report on the synthesis and characterization of a rigid 5,15-functionalized diphosphonic acid porphyrin, together with a procedure for the reproducible assembly of the porphyrin units into well-defined, multilayered thin films utilizing ZrP linkages. Previous work by Katz and co-workers [16,17] on surface-immobilized porphyrin/viologen phosphonate combinations should be noted, as should the work by Nixon et al. [18] on ZrP-linked Langmuir–Blodgett films of metalloporphyrins. For the films described here, soft lithography has been combined with the fabrication procedure to generate micropatterned versions of the assemblies. Micropatterning engenders interesting visible-light diffraction properties that are potentially useful in the context of chemical sensing [15]. It also permits film thicknesses to be evaluated directly by surface proximal probe microscopy techniques. We intend in a

* Corresponding author. Tel.: +1-847-491-3504; fax: +1-847-491-7713.
E-mail address: jthupp@chem.nwu.edu (J.T. Hupp).

0277-5387/$ - see front matter © 2003 Elsevier Ltd. All rights reserved.
doi:10.1016/S0277-5387(03)00428-5

subsequent report (work in progress) to describe the extension of the ZrP fabrication method to porphyrinic molecular squares [14,19] to yield very high porosity micro- and mesostructures.

2. Results and discussion

2.1. Synthesis

The MacDonald [2+2] synthetic strategy [20] was used to prepare substituted porphyrin **1** from 2,2′-dipyrrylmethane and diethyl-4-formylphenylphosphonate (Scheme 1). Both, 2,2′-dipyrrylmethane [21] and diethyl-4-formylphenylphosphonate [22], were synthesized according to standard literature procedures.

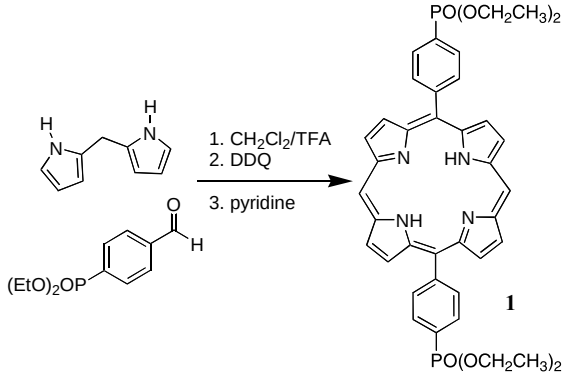

Scheme 1.

2.2. Zirconium phosphonate film assembly

The assembly procedure for mono- and multilayer films of **1**, shown schematically in Scheme 2, builds on methods described in the literature [7–9,23–26]. The deposition times for Zr(IV) and **1** were optimized to yield the greatest amount of **1** per synthesis cycle, as indicated by electronic absorption spectroscopy. Deposition times exceeding those described in Section 4 did not lead to additional porphyrin incorporation. Importantly, and consistent with previous work, a subsequent layer would not deposit until the sample was exposed to a solution of Zr(IV); this two-step assembly sequence is the basis for systematic control of film thickness. X-ray Photoelectron Spectroscopy (XPS) (results not shown) corroborate the addition of zirconium with each fabrication cycle.

2.3. Electronic absorption and emission spectroscopy

Molecule **1** is a highly absorbing ($\varepsilon_{402} = 2.5 \times 10^5$ M^{-1} cm^{-1}) chromophore (Fig. 1, solid line) and is fluorescent in unbuffered aqueous solution ($\Phi_{fl} = 0.07$) (Fig. 1, dashed line). Upon immobilization of **1** on a glass or indium tin oxide (ITO) surface via ZrP bond-formation (one assembly cycle), the porphyrin's Soret absorption band splits into a red-shifted band and a blue-shifted band (Fig. 1, dotted/dashed line). The splitting is characteristic of excitonic interactions arising from "edge-on-edge" porphyrin aggregate formation [27]. Electronic absorption spectra of thicker films prepared via multiple cycles through Scheme 2 also indicate a high degree of aggregation. Another signature of

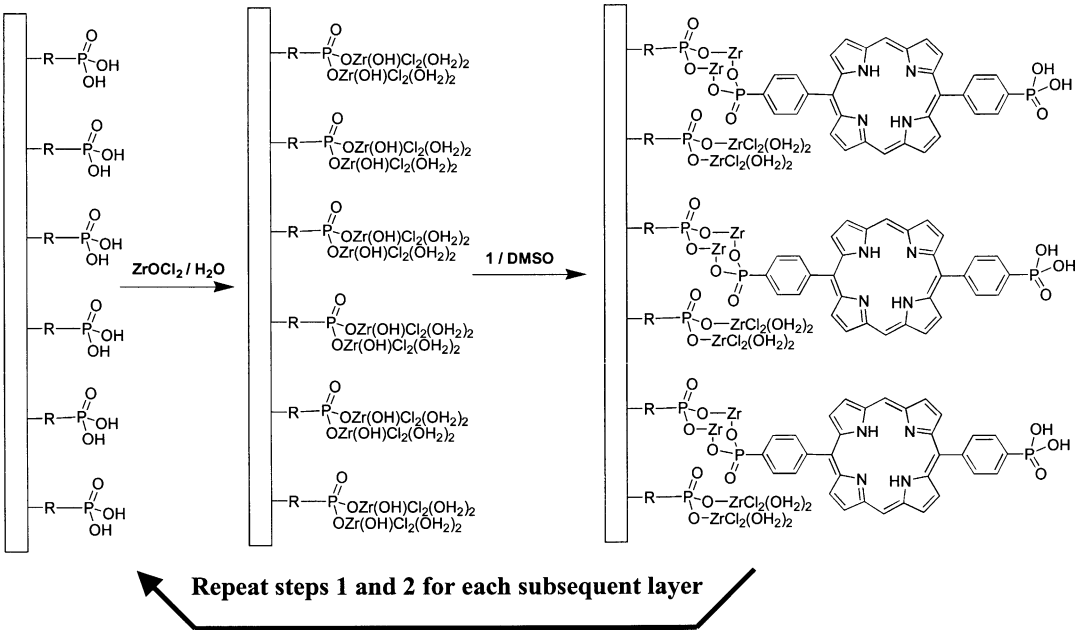

Scheme 2.

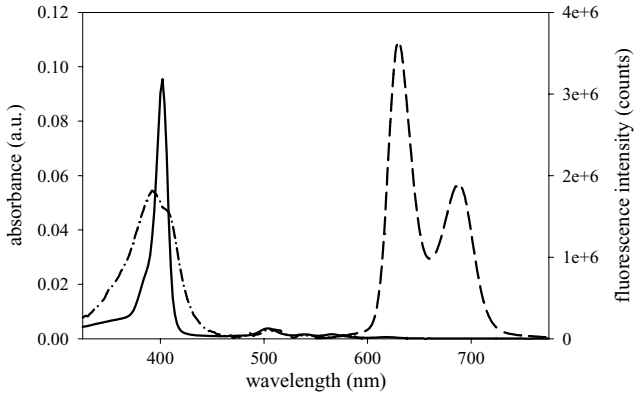

Fig. 1. Electronic absorption spectra of **1** in H_2O (0.4 μM) (solid line) and assembled in a ZrP film (2 layers) (dotted line). Also shown is the electronic emission spectrum of **1** in H_2O (0.4 μM) (dashed line).

porphyrin aggregation, also observed here, is a marked decrease in fluorescence quantum yield together with a decrease in emission lifetime [28–31].

A plot of the absorbance at 408 nm, as a function of the number of assembly cycles, is linear with an average absorbance increase of 0.04 per growth cycle, implying consistent cycle-to-cycle increases in porphyrin film thickness, Fig. 2. Since the films assemble on both sides of the platforms, the actual absorbance increase per film assembly cycle is 0.02. Assuming a 9 $\mathring{A} \times 5$ $\mathring{A}$ footprint per molecule [32], one molecular layer per cycle, and using the extinction coefficient of **1** in solution, a close-packed monolayer is calculated to have an absorbance of 0.09. The difference between calculated and measured absorbance changes can be partially accounted for by the fact that aggregated porphyrins often exhibit substantial reductions in extinction coefficient in the Soret region [33]. In addition, the edge-on-edge configuration suggests a less tightly packed arrangement, a conclusion supported by electrochemical redox-probe experiments described below. Attempts to densify the films through sonication or heating during deposition proved unsuccessful.

Cao et al. [7] have pointed out that films constructed from diphosphonic acid molecules featuring large footprints suffered from Zr(IV)–Zr(IV) lateral spacings that are too large to permit formation of continuous zirconium inter-layers such as those formed by inorganic metal phosphonates. Instead, Zr(IV) species likely form either isolated or paired linkages (see Scheme 2). Given the crystallographic precedent for the latter linkage [34], we speculate that the paired linkage is also formed here.

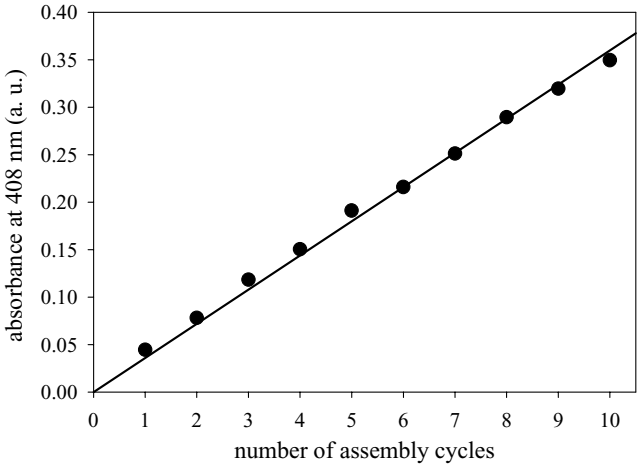

Fig. 2. Measured absorbance at 408 nm for thin films of **1** (normal to the incident light) as a function of the number of assembly cycles.

2.4. Polarized absorbance

Polarized absorbance measurements [35–37] were performed to determine the orientation of adsorbed **1** relative to the surface since oriented chromophores should display anisotropic absorption. In the following discussion, *x* and *y* axes define the plane of the sample, and the *z*-axis is normal to the surface. Experiments performed with films held normal to the incident plane polarized beam showed no anisotropy (Fig. 3). This indicates that the transition dipole moments are randomly oriented in the *x*–*y* plane of the film – a reasonable outcome given the film fabrication protocol. To determine whether porphyrin units are oriented with respect to the *z*-direction, samples were positioned at 45° to the incident beam, thereby rotating the *z*-axis into the sampling plane of the incident light. This configuration yields highly anisotropic absorption (Fig. 3), with the absorbance maximizing at 90° polarization. If the porphyrin transition dipole moment lies along the long axis of the molecule, which is a reasonable assumption, then the axial anisotropic absorption confirms that the porphyrin molecules are oriented normal to the surface.

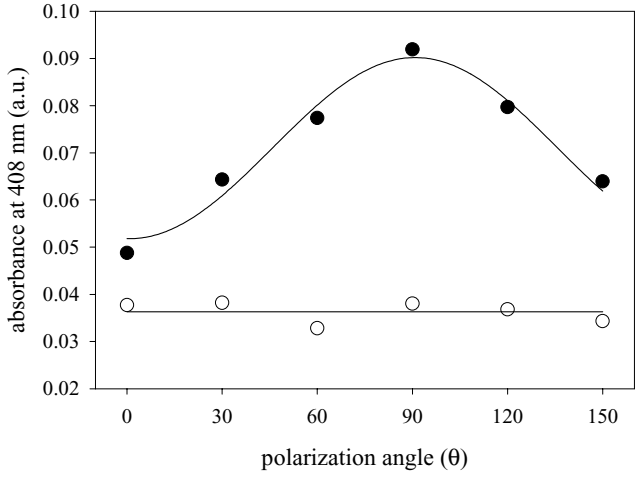

Fig. 3. Absorbance in the Soret region for a single layer thin film of **1** as a function of the polarization angle of the incident light. Shown are the data collected with the film surface normal to the incident light (open circles) and 45° to the incident light (filled circles).

2.5. Atomic force microscopy and micropatterning of porphyrin multilayers

Surface topographical characterization was performed using contact-mode atomic force microscopy (AFM). The RMS roughness of the bare ITO platforms used here is 2–3 nm, making the determination of film thicknesses difficult, especially when few molecular layers are analyzed. To circumvent this problem, ZrP films of **1** were micropatterned using a variant of "micromolding in capillaries" (MIMIC), a soft lithography technique developed by Whitesides and co-workers (see Section 4 for details) [38]. Fig. 4 shows that the patterns can be readily imaged by AFM, based on even a single assembly cycle. The MIMIC patterning process allows for film heights to be determined directly via AFM. The film heights as a function of the number of repetitive assembly cycles are shown in Fig. 5. This linear plot gives a thickness increase per assembly cycle of 2.1 nm, consistent with the addition of a single layer, one molecule thick (porphyrins oriented approximately normal to the surface), per cycle.

2.6. Diffraction of visible light

Micropatterning of thin films to form periodic structures makes the films capable of diffracting visible light [39,40], a property we have found useful in applications ranging from semiconductor band-edge determination [41] to chemical sensing [15,42–44]. In general, the efficiency of a grating is defined as the ratio of the light intensity diffracted into constructive interference spots to the incident light intensity. The diffraction efficiency (*DE*) of a periodic grating with the geometry of our micropatterned films should be well approximated by the following simplified expression [43]:

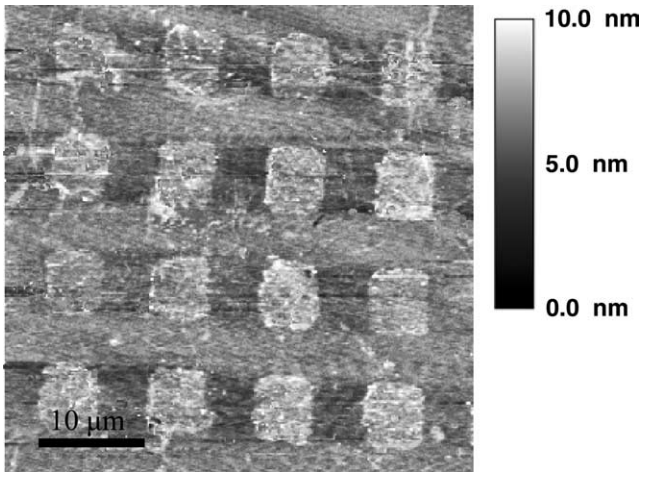

Fig. 4. An AFM image of a single micropatterned layer of **1**.

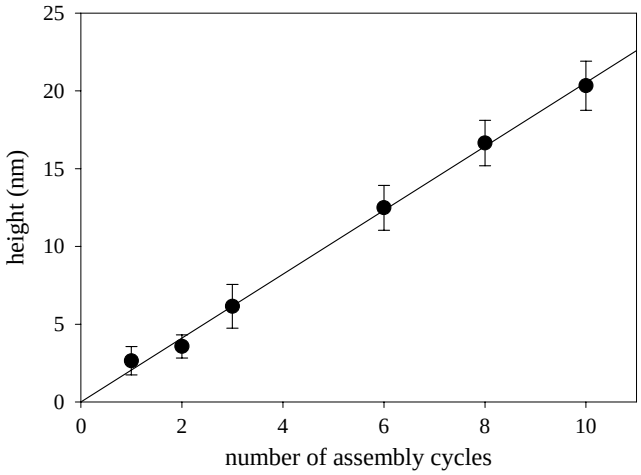

Fig. 5. Film heights of micropatterned thin films of **1** as a function of the number of assembly cycles as measured via AFM.

$$DE = 0.0253 \sin^2\left(\frac{2\pi(\tilde{n}_{\text{film}} - \tilde{n}_{\text{air}})d}{\lambda}\right), \quad (1)$$

where $\tilde{n}_{\text{film}}$ and $\tilde{n}_{\text{air}}$ are the complex refractive indices of the film and air, d is the film thickness, and λ is the wavelength of the incident light. Relative measures of grating efficiencies (in the low efficiency limit) are easily obtainable from the ratio of one constructive interference spot to the undiffracted beam. According to Eq. (1), for a fixed degree of refractive index contrast, the *DE* should be proportional to the square of the patterned film thickness, in the low *DE* limit. A single patterned layer of **1** produces a measurable diffraction pattern, and the efficiency of a pattern of three layers is considerably greater.

2.7. Electrochemical assessment of film porosity

The ability of thin films either to block or transport redox-active probe molecules can be readily discerned via electrochemical measurements if the films are prepared on conductive platforms [14,45]. We have performed slow-sweep voltammetry studies with ferrocene–methanol (Fc–MeOH; diameter ≈4.5 Å), osmium(II) (4,7-dimethyl-1,10-phenanthroline) $_2$(4-pyrrolidinopyridine)$_2^{2+}$ (Os(dmphen)$_2$(pypy)$_2^{2+}$; diameter ≈13.0 Å), and iron(II) tris-(bathophenanthroline sulfonate) (Fe(bphen)$_3^{4-}$; diameter ≈23.0 Å) as probes. As shown in Fig. 6, the two smaller probe molecules readily permeate ZrP-assembled porphyrin films three layers thick and undergo electrochemistry at the underlying conductive platform. The large probe, however, is essentially completely blocked by even a single layer of **1**. That the blockage is not a charge effect is shown by the ability of ferrocyanide to permeate the films (data not included in the figure). The combined experiments point to the existence of openings or pores several angstroms

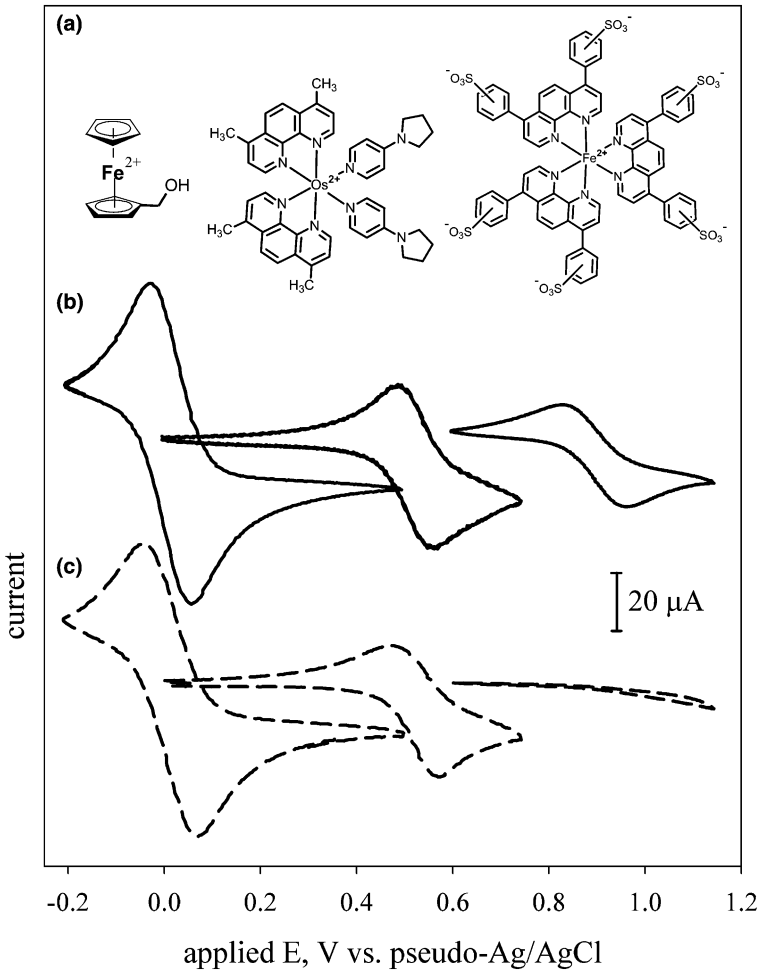

Fig. 6. (a) The three redox-probes used in this work (left to right): Fc–MeOH, $Os(dmphen)_2(pypy)_2^{2+}$, and $Fe(bphen)_3^{4-}$, and (b) their corresponding cyclic voltammograms (directly below their structure) using a bare ITO platform as the working electrode (solid lines) (all concentrations were 2 mM). (c) Cyclic voltammograms for Fc–MeOH and $Os(dmphen)_2(pypy)_2^{2+}$ using ITO with three layers of **1** as the working electrode (dashed lines) and a voltammogram for $Fe(bphen)_3$ using ITO with one layer of **1** as the working electrode.

in width in the mono- and multilayers. Work in progress is directed toward quantifying the film permeation rates and manipulating the chemical selectivity of the permeation process by decorating the film exterior with appropriate chemical and biochemical discriminators.

3. Conclusions

Consistent with earlier reports for a tetra-functionalized porphyrin [16,17], doubly phosphonate-functionalized porphyrins can be used to construct mono- and multilayer films via ZrP chemistry. Polarized absorption measurements show that the film-based porphyrins lack a net orientation in the *x*–*y* plane, but are highly oriented in the *z*-direction. Soft lithography techniques can be used to prepare micropatterned versions of the films which, in turn, permit film thicknesses to be evaluated directly via AFM measurements. The thicknesses increase uniformly with the number of assembly cycles. The micropatterned films also are capable of diffracting visible light, with the diffraction efficiency increasing with film thickness. Electrochemical measurements establish that the films are permeable toward small redox-probe molecules, but blocking toward larger species.

4. Experimental

Zirconyl chloride octahydrate, 2,4,6-collidine, boron-trifluoride etherate, 4-bromobenzaldehyde, ethylene glycol, *p*-toluenesulfonic acid, diethylphosphite, triethylamine, ferrocene–methanol, potassium ferrocyanide, and potassium nitrate were used as received from Aldrich. Anhydrous toluene, acetonitrile, diethyl ether, anhydrous magnesium sulfate, sodium carbonate, sulfuric acid, tetrahydrofuran and dimethyl sulfoxide (DMSO) were used as received from Fisher Scientific. 3-aminopropyltrimethoxysilane (APTMS) (United Chemical Technologies), phosphorous oxytrichloride ($POCl_3$) (Alfa Aesar),

pyrrole-2-carboxaldehyde (Lancaster), sodiumborohydride (Lancaster), tetrakis(triphenylphosphine)-palladium (STREM), and the sodium salt of iron(II)tris-bathophenanthrolinesulfonate (GFS) were used as received. [Osmium(II)(4,7-dimethyl-1,10-phenanthroline)$_2$ (4-pyrrolidinopyridine)$_2$]Cl_2 was prepared according to a literature procedure [46,47]. Pyrrole (Aldrich) was dried over KOH pellets overnight and freshly distilled from sodium metal immediately prior to use. Water was purified using a Millipore filtration and ion-exchange system (resistivity of 18.2 MΩ.)

UV–visible absorption measurements were performed on a Hewlett Packard HP8452A diode array spectrophotometer. Steady-state fluorimetry measurements were performed on a Jobin Yvon-SPEX Fluorolog-3 spectrofluorimeter. AFM measurements were performed using a Digital Instruments Bioscope AFM head and a Nanoscope IIIa controller. All measurements were obtained in contact-mode with Nanoprobe SPM tips (DNP-S20, Digital Instruments). Diffraction efficiency measurements were made on a homebuilt apparatus which has been described elsewhere in detail [42]. Electrochemical measurements were performed with a Bioanalytical Systems (BAS CV-27) potentiostat using a three-electrode configuration with an ITO working electrode, a Pt wire counter-electrode and a silver wire electrocoated with silver chloride (pseudo-Ag/AgCl) as the reference electrode. All redox-probe solutions were prepared in water and contained 2 mM probe concentrations together with 0.2 M KNO_3 (aq.) as the supporting electrolyte. A homebuilt cell was used to limit the analyzed region of each film (active working electrode area) to a 2.5 mm radius circle.

*4.1. Diethyl-4-[12-[4-(diethoxyphosphoryl)phenyl]-21,22,23,24-tetraazapentacyclo[16.2.1.1.1.1]tetracosa-1(21),2,4,6,8(23),9,11,13,15,17,19-undecaen-2-yl]phenylphosphonate (**2**)*

Dipyrryl methane (500 mg, 3.4 mmol), diethyl-4-formylphenylphosphonate (826 mg, 3.4 mmol), and freshly distilled methylene chloride (600 ml) was added to a 2-neck, 1-L flask equipped with a magnetic stir bar and a reflux condenser. The solution was deoxygenated via nitrogen bubbling for 10 min. Trifluoroacetic acid (165 μl, 2.14 mmol) was then added via syringe and the solution was heated to reflux under nitrogen for 7 h. 2,3-Dichloro-5,6-dicyano-1,4-benzoquinone (DDQ) (1 g, 4.40 mmol) was added to oxidize the porphyin and the mixture was refluxed for another hour. Next, pyridine (3.5 ml) was added to precipitate the DDQ while the mixture was refluxed for an additional hour. The solution was then cooled to room temperature and filtered. The filtrate was washed with water (5×200 ml) and a saturated, aqueous solution of sodium carbonate (2×200 ml) was dried over $MgSO_4$ and the solvent was removed by rotary evaporation to give a dark reddish-purple solid. To aid in the column purification, the solid was dissolved in a minimum amount of CH_2Cl_2 (10 ml) and precipitated into 400 ml of hexanes. The purple crystalline crude product was then isolated from the burgundy solution. Repeated precipitations in this manner (4×) greatly simplified subsequent column purification. The crude porphyrin was further purified by flash chromatography on silica gel column (98:2 CH_2Cl_2/MeOH) that had been wet-packed with 5% triethylamine in CH_2Cl_2 to prevent streaking of the porphyrin on the column. The desired porphyrin was isolated as a purple solid in a 19% yield (290 mg, 0.32 mmol). ^{1}H NMR (400 MHz, $CDCl_3$): δ − 3.14 (s, 2H), 1.57 (t, 12H, $J = 6.8$ Hz), 4.43 (m, 8H), 8.30 (m, 4H), 8.40 (m, 4H), 9.06 (d, 4H, $J = 4.4$ Hz), 9.44 (d, 4H, $J = 4.4$ Hz), 10.37 (s, 2H). ^{13}C NMR (500 MHz, $CDCl_3$): δ 146.91, 145.73, 145.56, 135.61 (d, $J = 15.4$ Hz), 132.32, 131.05, 130.57 (d, $J = 10.2$ Hz), 128.86, 127.36, 118.03, 105.97, 62.75 (d, $J = 5.1$ Hz), 16.82 (d, $J = 6.4$ Hz). UV–Vis ($CHCl_3$): λ_{max} (log ε) 408 (5.41), 502 (4.07), 538 (3.67), 574 (3.61), 628 nm (3.16). HRFABMS (NBA): Calc. for $C_{40}H_{41}N_4O_6P_2$ (MH^+): 735.2504. Found: 735.2501. *Anal.* Calc. for $C_{40}H_{40}N_4O_6P_2 \cdot 1.5\ H_2O$: C, 63.07; H, 5.69; N, 7.36. Found: C, 63.21; H, 5.51; N, 7.29%.

*4.2. 4-[12-(4-phosphonophenyl)-21,22,23,24-tetraazapentacyclo[16.2.1.1.1.1]tetracosa-1(21),2,4,6,8(23),9,11,13,15,17,19-undecaen-2-yl]phenylphosphonic acid (**1**)*

The diethyl ether diphosphonate porphyrin (**2**) (30 mg, 0.041 mmol) was dissolved in freshly distilled methylene chloride (10 ml) in a 50-ml Schlenk flask equipped with a magnetic stir bar and a reflux condenser. The resulting solution was deoxygenated with nitrogen for 5 min. Bromotrimethylsilane (86 μl, 0.66 mmol) was added via syringe and the mixture was stirred overnight at 40 °C under nitrogen. The solvent was then removed from the reaction mixture by rotary evaporation to give a dark solid that was stirred in water (10 ml) for 2 h. The reaction mixture was filtered and the resulting crude product was washed with water and hexanes to give a purple solid in 96% yield (24 mg, 0.039 mmol). ^{1}H NMR (400 MHz, DMSO-d_6): δ − 3.29 (s, 2H), 8.19 (m, 4H), 8.39 (m, 4 H), 9.04 (d, 4H, $J = 3.9$ Hz), 9.70 (d, 4H, $J = 3.9$ Hz), 10.69 (s, 2H). ^{13}C NMR (500 MHz, DMSO-d_6): δ 146.28, 144.96, 142.96, 134.58, 134.33, 133.03, 130.79, 129.54, 118.05, 106.15. UV–Vis (DMSO): 404 nm. HRFABMS (NBA): Calc. for $C_{32}H_{24}N_4O_6P_2$: 623.1250. Found: 623.1249.

4.3. ZrP-assembled porphyrin films

Glass and ITO (Delta Technologies, 10 Ω/square) platforms were cut to 0.9×3 cm, cleaned for 30 min in a

3:1 H_2SO_4: H_2O_2 solution (*Caution: this solution reacts violently with organic compounds*) [48], then rinsed with copious amounts of water and oven dried (70 °C, 15 min). The glass platforms were then primed with an amine-terminated monolayer via overnight soaking in 1% v/v APTMS in dry toluene. The primed glass surface was then phosphorylated according to a previous method [8] in a 1:1 solution of 2,4,6-collidine (20 mM) and $POCl_3$ (20 mM) in anhydrous acetonitrile for 30 min. The ITO platforms were phosphorylated in the same manner, but without a priming layer [8]. The phosphonate-terminated samples were then exposed to tetravalent zirconium by an overnight soak in 25 mM $ZrOCl_2 \cdot 8H_2O$ (aq.). A subsequent 4 h soak in a solution of **1** (0.01 mM in DMSO) in the dark completed the first zirconium phosphonate (porphyrin) layer. After each Zr(IV) or porphyrin exposure, the resulting platforms were rinsed by soaking in clean H_2O and DMSO, for 10 min each. Additional ZrP porphyrin layers were assembled through successive treatment with 25 mM $ZrOCl_2$ (15 min) and 0.01 mM porphyrin (4 h) in the dark. All samples were stored in the dark in a vacuum desiccator before usage.

4.4. Polarized electronic absorption

Platforms were cut to 1.3×3.0 cm to ensure 45° positioning in a 1 cm cuvette, and films were assembled by the above procedure. A plane polarizer (Melles Griot, 03FPG003) was placed in the incident light beam of the spectrophotometer and was rotated to the desired angle. For 45° measurements, a baseline measurement was recorded at each polarization angle with a 1.3×3.0 cm platform which had been cleaned, primed, phosphorylated, and zirconated. The baseline signal was then subtracted from the signals from layered samples to eliminate error due to differences in reflectance with different light polarizations. After all data were collected at 45° incident angle, the platform was carefully cut to 0.9×3.0 cm and polarized absorption measurements were taken at normal light incidence. A 0.9×3.0 cm blank platform was used to collect the baseline for each polarization angle.

4.5. Micropatterning of ZrP multilayers

Micropatterning of **1** was achieved through an extension of the soft lithography technique known as micromolding in capillaries [38]. Using a previously described method [49], polydimethylsiloxane (PDMS) stamps for microtransfer molding were fabricated by curing a 10:1 mixture of elastomer-hardener (Sylgard Silicone 184, Dow Corning) over commercially obtained lithographic master (10 μm pitch) (AFM) calibration grating (Digital Instruments) with etched square features approximately 185 nm deep, and laterally measuring 5 μm × 5 μm with a lattice constant of 10 μm. The PDMS was cured at room temperature for 1 h, followed by additional curing at 60 °C for 1 h. The PDMS stamp was placed in contact with cleaned, phosphorylated, and zirconated glass or ITO platforms. A 1:4 mixture of photoresist (AZ1518) and acetone was carefully pipetted near the stamp edge and was drawn underneath the stamp via capillary action. The photoresist was cured at 60 °C for 15 min and the stamp was carefully pealed from the platform. The deposition solvent for all micropatterns was water since DMSO dissolves the photoresist mask. Multilayer assembly was performed as described above. Following layer assembly, the photoresist mask was removed by soaking in acetone for 10 min.

Acknowledgements

We thank Jose Lozano at the Center for Materials Chemistry, Department of Chemistry and Biochemistry, University of Texas at Austin for XPS measurements. We thank the US Dept. of Energy (Grant No. DE-FG02-01ER15244) and the Camille and Henry Dreyfus Postdoctoral Program in Environmental Chemistry (fellowship for RWG) for financial support.

References

[1] M. Ferreira, J.H. Cheung, M.F. Rubner, Thin Solid Films 244 (1994) 806.
[2] V.L. Colvin, M.C. Schlamp, A.P. Alivisatos, Nature 370 (1994) 354.
[3] J.H. Cheung, A.F. Fou, M.F. Rubner, Thin Solid Films 244 (1994) 985.
[4] H.E. Katz, G. Scheller, T.M. Putvinski, M.L. Schilling, W.L. Wilson, C.E.D. Chidsey, Science 254 (1991) 1485.
[5] D. Li, M.A. Ratner, T.J. Marks, C.H. Zhang, J. Yang, G.K. Wong, J. Am. Chem. Soc. 112 (1990) 7389.
[6] N. Tillman, A. Ulman, T.L. Penner, Langmuir 5 (1989) 101.
[7] G. Cao, H.-G. Hong, T.E. Mallouk, Acc. Chem. Res. 25 (1992) 420.
[8] H.E. Katz, M.L. Schilling, C.E.D. Chidsey, T.M. Putvinski, R.S. Hutton, Chem. Mater. 3 (1991) 699.
[9] J.L. Snover, H. Byrd, E.P. Suponeva, E. Vicenzi, M.E. Thompson, Chem. Mater. 8 (1996) 1490.
[10] H.-G. Hong, T.E. Mallouk, Langmuir 7 (1991) 2362.
[11] D.L. Feldheim, K.C. Grabar, M.J. Natan, T.E. Mallouk, J. Am. Chem. Soc. 118 (1996) 7640.
[12] D.M. Kaschak, T.E. Mallouk, J. Am. Chem. Soc. 118 (1996) 4222.
[13] D.M. Kaschak, J.T. Lean, C.C. Waraksa, G.B. Saupe, H. Usami, T.E. Mallouk, J. Am. Chem. Soc. 121 (1999) 3435.
[14] M.E. Williams, J.T. Hupp, J. Phys. Chem. 105 (2001) 8944.
[15] G.A. Mines, B. Tzeng, K.J. Stevenson, J. Li, J.T. Hupp, Angew. Chem. 41 (2002) 154.
[16] S.B. Ungashe, W.L. Wilson, H.E. Katz, G.R. Scheller, T.M. Putvinski, J. Am. Chem. Soc. 114 (1992) 8717.
[17] H.E. Katz, Chem. Mater. 6 (1994) 2227.

[18] C.M. Nixon, K. LeClaire, F. Odobel, B. Bujoli, D.R. Talham, Chem. Mater. 11 (1999) 965.
[19] R.V. Slone, J.T. Hupp, Inorg. Chem. 36 (1997) 5422.
[20] G.P. Arsenault, E. Bullock, S.F. MacDonald, J. Am. Chem. Soc. 82 (1960) 4384.
[21] R. Chong, P.S. Clezy, A.J. Liepa, A.W. Nichol, Aust. J. Chem. 22 (1969) 229.
[22] D. Deniaud, B. Schöllorn, D. Mansuy, J. Rouxel, P. Battioni, B. Bujoli, Chem. Mater. 7 (1995) 995.
[23] M.L. Schilling, H.E. Katz, S.M. Stein, S.F. Shane, W.L. Wilson, S. Buratto, S.B. Ungashe, G.N. Taylor, T.M. Putvinski, C.E.D. Chidsey, Langmuir 9 (1993) 2156.
[24] S.F. Bent, M.L. Schilling, W.L. Wilson, H.E. Katz, A.L. Harris, Chem. Mater. 6 (1994) 122.
[25] M.M. Fang, D.M. Kaschak, A.C. Sutorik, T.E. Mallouk, J. Am. Chem. Soc. 119 (1997) 12184.
[26] J.C. Horne, G.J. Blanchard, J. Am. Chem. Soc. 118 (1996) 12788.
[27] M. Kasha, H.R. Rawls, M.A. El-Bayoumi, Pure Appl. Chem. 11 (1965) 371.
[28] S.B. Brown, M. Shillcock, P. Jones, Biochem. J. 153 (1976) 279.
[29] J. Lavorel, J. Phys. Chem. 61 (1957) 1600.
[30] R. Margalit, N. Shaklai, S. Cohen, Biochem. J. 209 (1983) 547.
[31] A.P.H.J. Schenning, D.H.W. Hubert, M.C. Feiters, R.J.M. Nolte, Langmuir 12 (1996) 1572.
[32] S.J. Silvers, A. Tulinsky, J. Am. Chem. Soc. 89 (1967) 3331.
[33] J.W. Weigl, J. Mol. Spectrosc. 1 (1957) 216.
[34] B. Zhang, D.M. Poojary, A. Clearfield, Inorg. Chem. 37 (1998) 249.
[35] K. Aramata, M. Kamachi, M. Takahashi, A. Yamagishi, Langmuir 13 (1997) 5161.
[36] R. Azumi, M. Matsumoto, Y. Kawabata, S. Kuroda, M. Sugi, L.G. King, M.J. Crossley, J. Phys. Chem. 97 (1993) 12862.
[37] M. Yoneyama, M. Sugi, M. Saito, K. Ikegami, S. Kuroda, S. Iizima, Jpn. J. Appl. Phys. 25 (1986) 961.
[38] E. Kim, Y.N. Xia, G.M. Whitesides, J. Am. Chem. Soc. 118 (1996) 5722.
[39] K.S. Schanze, T.S. Bergstedt, B.T. Hauser, C.S.P. Cavalaheiro, Langmuir 16 (2000) 795.
[40] K.S. Schanze, T.S. Bergstedt, B.T. Hauser, Adv. Mater. 8 (1996) 531.
[41] X. Dang, A.M. Massari, J.T. Hupp, Electrochem. Solid State Lett. 3 (2000) 555.
[42] A.M. Massari, K.J. Stevenson, J.T. Hupp, J. Electroanal. Chem. 500 (2001) 185.
[43] R.C. Bailey, J.T. Hupp, J. Am. Chem. Soc. 124 (2002) 6767.
[44] R.C. Bailey, B.C. Tzeng, X. Dang, G.A. Mines, K.A. Walters, J.T. Hupp, Electrochem. Soc. Proc. (2001) 511.
[45] A.G. Ewing, B.J. Feldman, R.W. Murray, J. Phys. Chem. 89 (1985) 1263.
[46] D.A. Gaal, J.T. Hupp, J. Am. Chem. Soc. 122 (2000) 10956.
[47] E.M. Kober, J.V. Caspar, B.P. Sullivan, T.J. Meyer, Inorg. Chem. 27 (1988) 4587.
[48] D.A. Dobbs, R.G. Bergman, K.H. Theopold, Chem. Eng. News 68 (1990) 2.
[49] K.J. Stevenson, J.T. Hupp, Electrochem. Solid State Lett. 2 (1999) 497.